R. E. Gibbs, P. Kotzer, and R. Piserchio, *Particles and Fields—1973*, edited by H. H. Bingham, M. Davier, and G. R. Lynch (A.I.P., New York, 1973).
[27]J. Hebert *et al.*, Barcelona-Batavia-Belgrade-Bucharest-Lund-Lyon-McGill-Nancy-Ottawa-Paris-Quebec-Rome-Valencia collaboration (unpublished).
[28]P. M. Fishbane and J. S. Trefil, Phys. Rev. D 9, 168 (1974).

PHYSICAL REVIEW D VOLUME 10, NUMBER 3 1 AUGUST 1974

Measurement of the magnetic moment and of the decay parameters of the Ξ^- hyperon*

R. L. Cool,† G. Giacomelli,‡ E. W. Jenkins,§ T. F. Kycia,
B. A. Leontic,‖ K. K. Li, and J. Teiger¶
Brookhaven National Laboratory, Upton, New York 11973
(Received 24 April 1974)

A measurement of the magnetic moment and of the decay parameters of the Ξ^- hyperon is reported. The measurement gave $\mu_\Xi = (-2.1 \pm 0.8)$ nuclear magnetons, corresponding to a gyromagnetic ratio of $g_\Xi = 4.2 \pm 1.6$. The measured Ξ^- decay parameters are $\alpha_\Xi = -0.39 \pm 0.05$, $\beta_\Xi = 0.08 \pm 0.26$, $\gamma_\Xi = 0.92 \pm 0.03$ ($\phi_\Xi = 5° \pm 16°$); and the lifetime $\tau_\Xi = (1.637 \pm 0.050) \times 10^{-10}$ sec. In the accepted angular range for the production of the Ξ^- (about $4.2° < \theta_{\rm lab} < 11.5°$) in the reaction $K^- + p \to K^+ + \Xi^-$, the polarization of the Ξ^- is 0.29 ± 0.10, 0.44 ± 0.09, 0.36 ± 0.10, and 0.21 ± 0.06 at laboratory momenta of 1.74, 1.80, 1.87, and 1.83 GeV/c, respectively.

I. INTRODUCTION

The measurement of the magnetic moment of a particle can provide a test of the validity of a theory. Such tests have been applied to quantum electrodynamics by measuring the magnetic moments of the electron and of the muon. The agreement between theory and experiment was found to be quite striking.

The magnetic moments of the baryons can be used to test the validity of the strong-interaction theories, in particular of unitary-symmetry theories. They could also give evidence for or against the various models for the fundamental triplets. Figure 1 shows the members of the $\frac{1}{2}^+$ baryon octet. SU(3) symmetry predicts that, apart from mass corrections, the members of the various U-spin multiplets have the same magnetic moment. The relation among the magnetic moments of the octet is given by[1]

$$\mu = \mu_2 - \mu_1 Q - \mu_2 [\, U(U+1) - \tfrac{1}{4} Q^2], \tag{1}$$

where Q is the charge and U is the U-spin. μ_2 and μ_1 may be determined from the known magnetic moments of the proton μ_p and of the neutron μ_n as

$$\mu_p = \tfrac{1}{2}\mu_2 - \mu_1 \tag{2}$$

and

$$\mu_n = -\mu_2 . \tag{3}$$

As a consequence, (1) predicts the values of the magnetic moments of the other members on the octet. In particular, the magnetic moment of the Ξ^- hyperon in units of nuclear magnetons ($\mu_N = e\hbar/2m_p c = 3.153 \times 10^{-18}$ MeV/c) is then predicted to be

$$\mu_\Xi = -(\mu_n + \mu_p) = -0.88 \mu_N . \tag{4}$$

The method of measuring the magnetic moment of the Ξ^- is that of determining the angle of precession of the Ξ^- polarization vector after passing through a strong magnetic field.[2] The Ξ^- hyperons are produced in the reaction

$$K^- + p \to \Xi^- + K^+ , \tag{5}$$

which acts as the polarizer. The polarization vector is perpendicular to the plane of production of the Ξ^- and therefore perpendicular to the Ξ^- direction.

The Ξ^- passes through a strong magnetic field which is essentially parallel to the Ξ^- momentum and therefore perpendicular to the Ξ^- magnetic moment (see Fig. 2). With this arrangement the Ξ^- track does not curve appreciably in the magnetic field.

In the Ξ^- rest frame the equation of motion of the polarization vector $\hat{\sigma}_\Xi$ in a magnetic field $\vec{\mathbf{H}}$ is

$$\frac{d\hat{\sigma}_\Xi}{dt} = \frac{\mu_\Xi}{s_\Xi \hbar} \hat{\sigma}_\Xi \times \vec{\mathbf{H}} , \tag{6}$$

where μ_Ξ and $s_\Xi \hbar$ are respectively the magnetic moment and the spin of the Ξ^-. By integrating

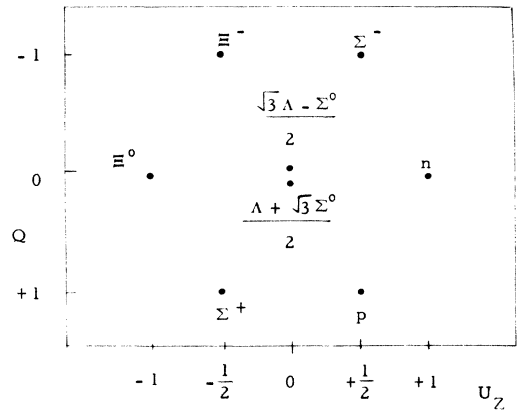

FIG. 1. The baryon spin-$\frac{1}{2}^+$ octet.

(6), keeping in mind that $\hat{\sigma}_\Xi$ and $\vec{H}$ are essentially perpendicular, one has for the angle of precession ϵ

$$\epsilon = (Hl)\left(\frac{\mu_\Xi}{s_\Xi}\right)\left(\frac{m_\Xi}{p_\Xi}\right), \tag{7}$$

where m_Ξ and p_Ξ are respectively the mass and the momentum of the Ξ^-; (μ_Ξ/s_Ξ) is the gyromagnetic ratio and (Hl) is the field integral along the Ξ^- trajectory. The final polarization direction is measured via the angular distributions of the parity-violating weak decays

$$\Xi^- \to \Lambda + \pi^- \qquad \Lambda \to p + \pi^- \tag{8}$$

which act as an analyzer. In our apparatus a Ξ^- with a magnetic moment of one nuclear magneton would precess through an angle of about 20°.

Technically the measurement of the magnetic moment of the Ξ^- is a difficult one because of the (i) small production cross section of reaction (5), (ii) small polarization of the Ξ^- in reaction (5), (iii) short lifetime of the Ξ^-, (iv) relatively small decay parameter α_Ξ, (v) low available K^- fluxes, and (vi) relatively small magnetic fields available for precessing the spin.

We report here a measurement of the Ξ^- magnetic moment performed at the Brookhaven Alternating Gradient Synchrotron (AGS). We also obtained data on the decay parameters and on the polarization of the Ξ^- in reaction (5). Preliminary results were published in a letter.[3] The notation for the Ξ^- decay parameters is defined in Sec. II, the experimental details are discussed in Sec. III, the experimental procedure in Sec. IV, the results in Sec. V, discussion and conclusion in Sec. VI.

II. Ξ^- DECAY PARAMETERS

In the following we shall assume that the spin of the Ξ^- is $\frac{1}{2}$. The decay parameters observed in the $\Xi^- \to \Lambda + \pi^-$ decay are defined as follows[4]:

$$\alpha_\Xi = \frac{2\,\mathrm{Re}S^*P}{|S|^2 + |P|^2}, \tag{9}$$

$$\beta_\Xi = \frac{2\,\mathrm{Im}S^*P}{|S|^2 + |P|^2}, \tag{10}$$

$$\gamma_\Xi = \frac{|S|^2 - |P|^2}{|S|^2 + |P|^2}, \tag{11}$$

where S and P are the amplitudes for the S and P waves in the $\Lambda\pi^-$ interaction. α_Ξ, β_Ξ, and γ_Ξ are related by

$$\alpha_\Xi^2 + \beta_\Xi^2 + \gamma_\Xi^2 = 1. \tag{12}$$

One also defines $\phi_\Xi = \arctan(\beta_\Xi/\gamma_\Xi)$. In the rest systems of the decaying Ξ^-, Λ and in the absence of external magnetic fields all decay angular distributions take the form

$$I(\theta) \propto (1 + A\cos\theta), \tag{13}$$

where θ is the angle between two appropriately chosen vectors, and A is a function of decay parameters and Ξ^- polarization.

Explicitly, the following distributions are considered in the decay chain (8) (see Fig. 2):

(a) distribution of the direction of the Λ momentum with respect to the Ξ^- polarization direction in the Ξ^- rest frame:

$$I_1 \propto 1 + \alpha_\Xi \overline{P}(\hat{\Lambda}\cdot\hat{\sigma}_\Xi)_\Xi, \tag{14}$$

where $\hat{\Lambda}$ and $\hat{\sigma}_\Xi$ are respectively unit vectors along the Λ momentum and the Ξ^- polarization directions; the Ξ subscript indicates that the angle has to be computed in the Ξ^- rest frame; $\overline{P}$ is the average

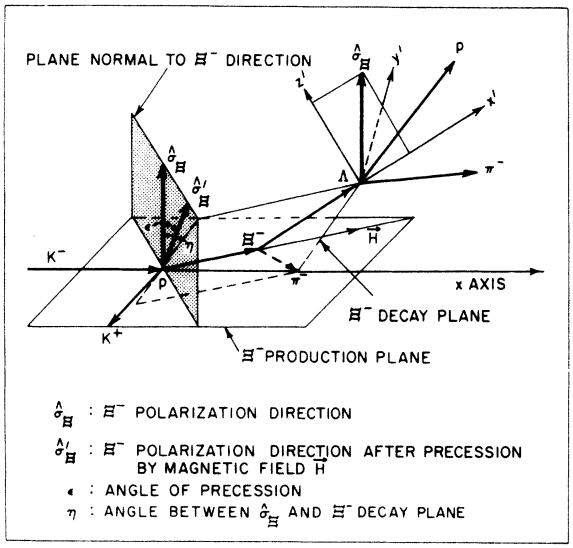

FIG. 2. Illustration of the relative orientations of the Ξ^- spin, the magnetic field, the Ξ^- momentum, and the Ξ^- cascade decay geometry.

Ξ^- polarization at production;

(b) distribution of the direction of the proton with respect to the Λ momentum direction (x' axis in Fig. 2) in the Λ rest frame:

$$I_2 \propto 1 + \alpha_\Lambda \alpha \ (\hat{p} \cdot \hat{\Lambda})_\Lambda ; \tag{15}$$

this is the only distribution which is independent of $\overline{P}$;

(c) distribution of the direction of the proton with respect to $(\hat{\sigma}_\Xi \times \hat{\Lambda})$ direction (y' axis in Fig. 2) in the Λ rest frame:

$$I_3 \propto 1 + \tfrac{1}{4}\pi \alpha_\Lambda \beta_\Xi \overline{P} (\hat{p} \cdot \hat{y}')_\Lambda , \tag{16}$$

where

$$\hat{y}' \equiv \frac{\hat{\sigma}_\Xi \times \hat{\Lambda}}{|\hat{\sigma}_\Xi \times \hat{\Lambda}|} ;$$

(d) distribution of the direction of the proton with respect to $[\hat{\Lambda} \times (\hat{\sigma}_\Xi \times \hat{\Lambda})]$ direction (z' axis in Fig. 2) in the Λ rest frame:

$$I_4 \propto 1 + \tfrac{1}{4}\pi \alpha_\Lambda \gamma_\Xi \overline{P} (\hat{p} \cdot \hat{z}')_\Lambda , \tag{17}$$

where

$$\hat{z}' \equiv \hat{\Lambda} \times \hat{y}' ;$$

(e) distribution of the direction of the proton with respect to the Ξ^- polarization direction $\hat{\sigma}_\Xi$ in the Λ rest frame:

$$I_5 \propto 1 + \tfrac{1}{3}(1 + 2\gamma_\Xi) \alpha_\Lambda \overline{P} (\hat{p} \cdot \hat{\sigma}_\Xi)_\Lambda . \tag{18}$$

Of the four equations (15)–(18), where the α_Λ parameter appears, only three are independent. In practice we have data without field and with field in opposite directions and we make simultaneous use of all the information to get the best value of α_Ξ, β_Ξ, γ_Ξ, $\overline{P}$, and μ_Ξ.

III. EXPERIMENTAL EQUIPMENT

Measurements of the Ξ^- polarization were carried out at 1.74, 1.80, and 1.87 GeV/c with the arrangement shown in Fig. 3; subsequently data on the magnetic moment of the Ξ^- were taken at 1.83 GeV/c with the arrangement shown in Fig. 4.

The incoming beam was defined by a two-counter telescope (S_1S_2), and the K^- mesons were identified by a liquid differential Čerenkov counter. The Ξ^- hyperons were produced in reaction (5) in the hydrogen target with the K^- mesons incident from the left. The apparatus was arranged to accept Ξ^-

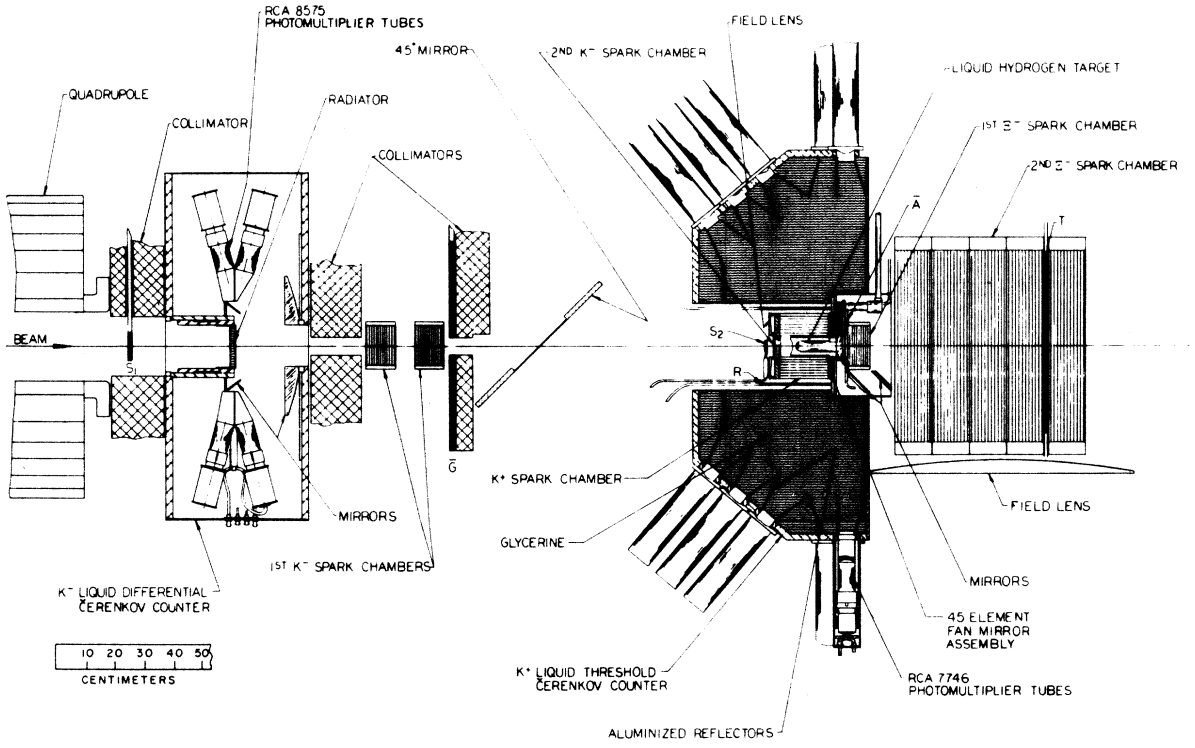

FIG. 3. Layout of the Ξ^- polarization measurements (without magnet) at 1.74, 1.80, and 1.87 GeV/c. S_1, $\overline{G}$, S_2, R, $\overline{A}$, T are scintillation counters. Also shown are the liquid differential Čerenkov counter used to select the incoming K^-, and the K^+ detector to select the K^+ decays into fast particles. The first and second K^- spark chambers were used to measure the incoming K^- direction, the cylindrical K^+ spark chamber to detect the outgoing K^+, and the first and second Ξ^- spark chambers to detect the Ξ^- production and the Ξ^- and Λ decays.

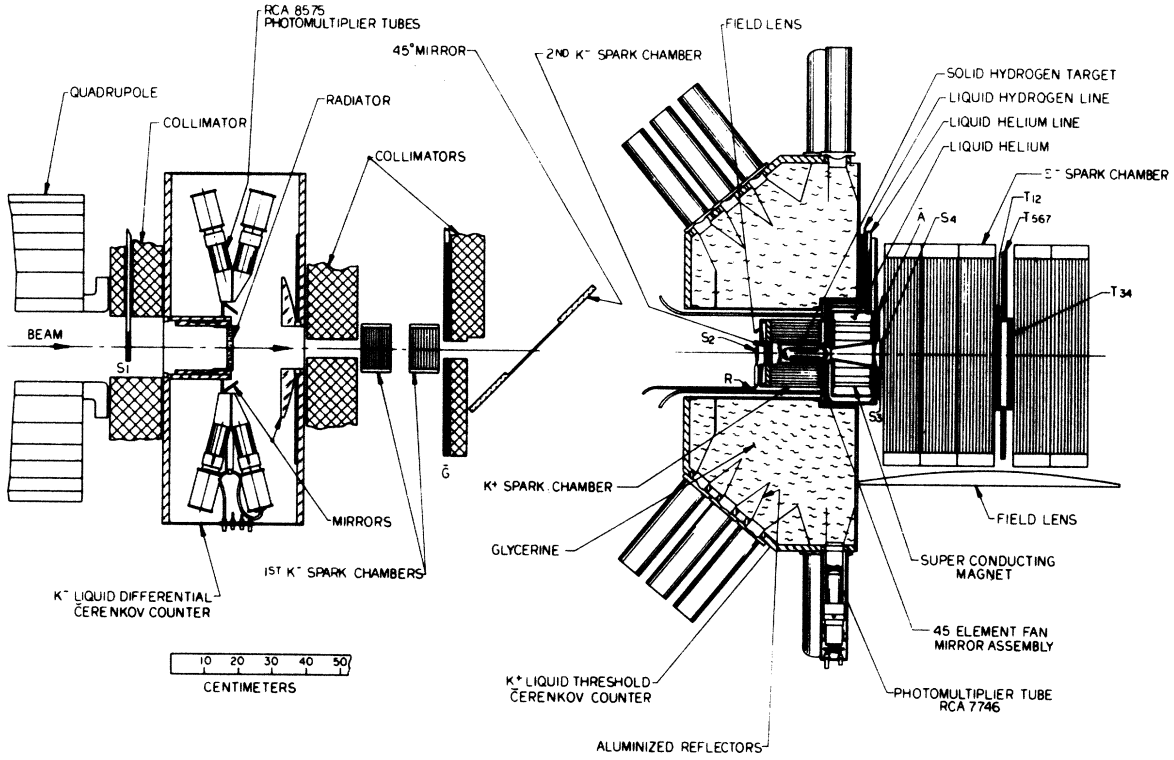

FIG. 4. Layout of the Ξ^- magnetic moment measurement (with the superconducting magnet). The notation is the same as that of Fig. 3. The layout differs in the addition of the superconducting magnet, in the presence of the dE/dx counters S_3, S_4, and in a modified T-counter arrangement.

produced forward in association with the K^+ emitted in the laboratory angular region between 75° and 120°. The K^+ mesons were detected by the cylindrical scintillation counter R and stopped in the liquid threshold Čerenkov counter which detected the K^+ by its fast decay products. The electronic detection of the Ξ^- was very loose and was carried out with scintillation counters. A more detailed description of the equipment follows.

A. Beam

The experiment was carried out in the partially separated beam 5B (Ref. 5) at the AGS. The beam layout is shown in Fig. 5. It viewed the $G10$ internal target at a 10° production angle. The target consisted of a 0.040-in.-diameter beryllium wire 0.60 in. in length, with the axis of the wire aligned along the beam direction.

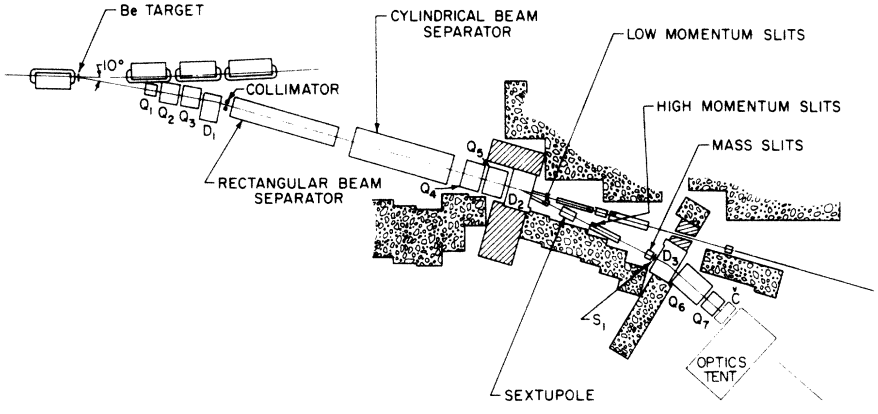

FIG. 5. Beam layout.

The first elements consisted of a quadrupole triplet, Q_1, Q_2, and Q_3, which provided a beam near parallel vertically and slightly converging horizontally through the separators. The bending magnet D_1 deflected particles of the desired momentum by 6° through the separators. The two electrostatic separators were 15 ft long with a 4-in. vertical gap and 8-in. horizontal aperture used in series and operated at between 400 and 500 kV. The quadrupole doublet Q_4 and Q_5 focussed the beam, after it was deflected by 12° by D_2, to a horizontal focus at the sextupole and to a vertical focus at the mass slit. Staggered collimators upstream and downstream from the sextupole, which partially corrected for chromaticity and narrowed the image at the mass slit, defined the momentum acceptance which was set at $\Delta p/p = \pm 2\%$. The third bending magnet D_3, by bending the beam by 13.5°, recombined particles of different momenta. The quadrupole doublet Q_6 and Q_7 focussed the beam to a final image of 1.1-in. diameter. The observed flux at 1.80 GeV/c was about 3×10^4 K^- per 10^{12} internal protons.

B. K^- Detector

The K^- mesons were identified by a liquid differential Čerenkov counter.[6] It had a 2-cm-thick radiator of perfluoro dimethyl cyclobutane (C_6F_{12}) with an index of refraction of 1.262, in a cell with thin quartz windows. Čerenkov light emitted by the K^- (Fig. 6) was focussed to a ring image by the reflecting lens, which also corrected for the chromaticity of the radiator. A conical mirror reflected the Čerenkov light radially to light guides which funnelled the light to RCA 8575 photomultipliers.

Čerenkov light from π mesons, muons and electrons was emitted at larger Čerenkov angles and was detected by a second set of RCA 8575 photomultipliers whose signal was used in anticoincidence. Nine photomultipliers were used in each of the two channels. The light guide and photomultiplier assembly could be moved remotely by a selsyn motor along the axis of the Čerenkov counter to center the K^- Čerenkov light on the narrow diaphragm.

The signals from the nine photomultipliers in the coincidence channel were mixed in groups of four and five to provide two signals between which a coincidence was required (C). The signals from the nine photomultipliers in the anticoincidence channel were added linearly and that sum signal ($\bar{C}$) was used in anticoincidence. The two Čerenkov counter signals were combined with the coincidence (S) between S_1 and S_2 scintillation counters to provide the K^- telescope signal ($SC\bar{C}$).

A "β" curve, shown in Fig. 7, was obtained for the two cases when the separated beam was tuned

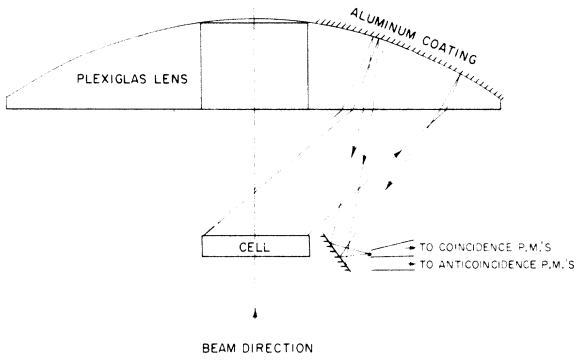

FIG. 6. Optics of the liquid differential Čerenkov counter.

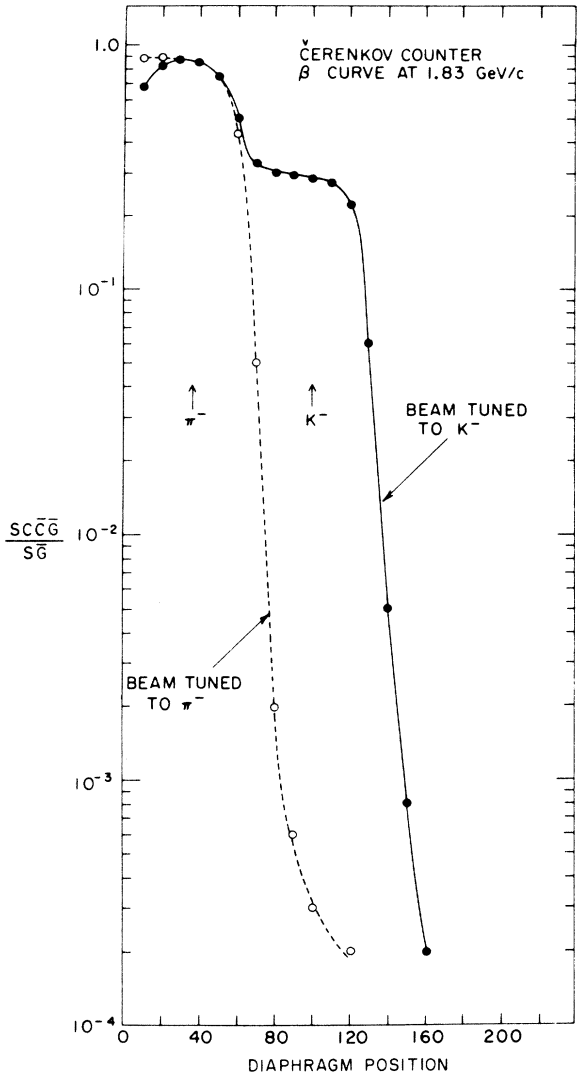

FIG. 7. Differential Čerenkov counter β curve at 1.83 GeV/c.

to K^- mesons and π^- mesons. It shows that when both the separated beam and the Čerenkov counter were tuned to K^-, the background due to π^- was about $\frac{1}{1000}$. The efficiency of the Čerenkov counter exceeded 90%.

C. Hydrogen target

The hydrogen target was a cylinder, 11 cm long and 4 cm in diameter. For the field-on data a solid hydrogen target was used. This was achieved by slowly solidifying hydrogen gas in the target, which was thermally connected to the helium reservoir by means of a plastic keel (see Fig. 8). A solid hydrogen target at liquid helium temperature has a density about 20% larger than a liquid one. Moreover, this was the simplest technical solution in our experimental arrangement with the superconducting magnet.

D. Precession magnet

The precession magnet was a superconducting solenoid. The advantages of using a superconducting magnet over a conventional pulsed one[2] are mainly connected with having a dc field so that one is not limited by beam spill. It was wound with about 8000 meters of niobium-tin (Nb_3Sn) ribbon from RCA.[7] The bore, which was shaped like a truncated cone, was 15 cm long, with diameters of the two bases of 4.5 and 8 cm, respectively. It was centered on the beam line with the vertex of the cone being at the center of the hydrogen target. The total length of the magnet plus walls and vacuum was approximately equal to two Ξ^- mean lives, which corresponds to the optimum situation. The maximum field achieved with the magnet was 122 kG at a position on the axis near the smaller cross section. In practice the magnet was charged up to

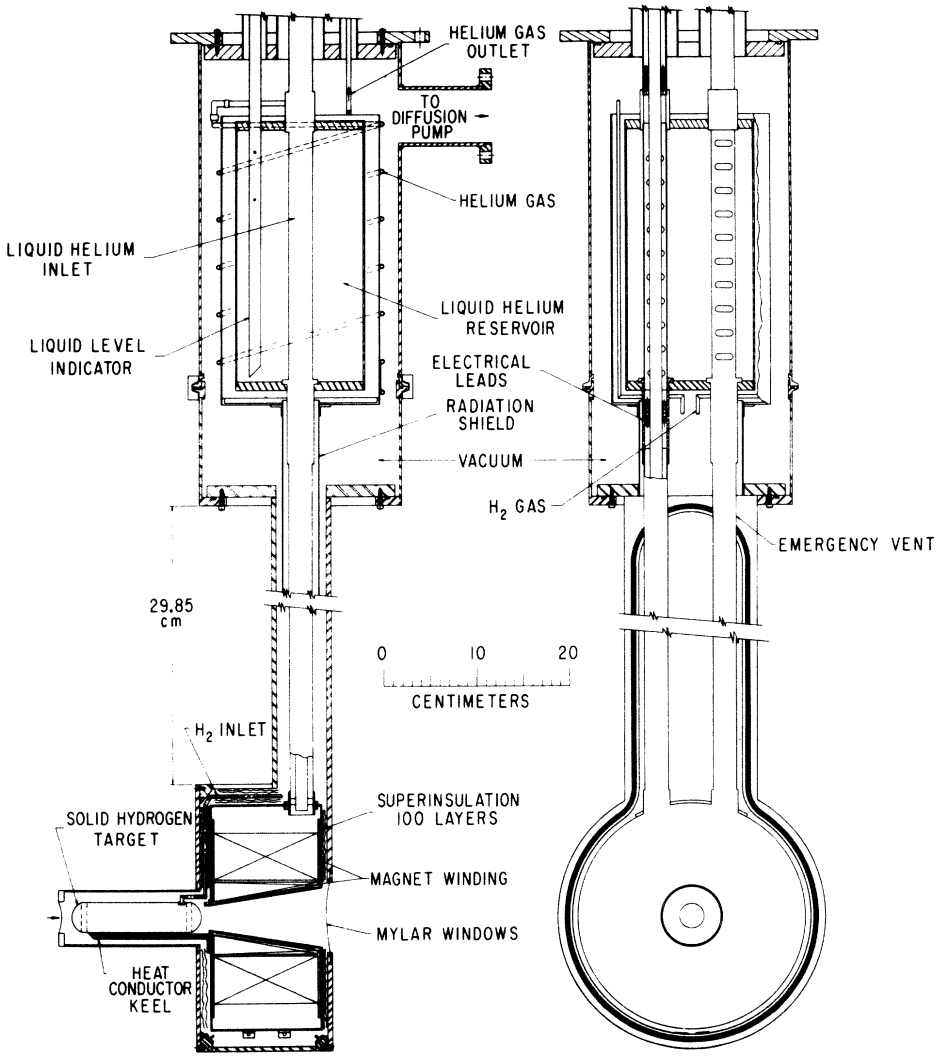

FIG. 8. Schematic diagram of the solid hydrogen target, superconducting solenoid, and liquid helium vessel.

about 118 kG; the magnetic field slowly decayed, with a loss of about 0.2 kG/hour, due to imperfect soldering joints. When the field reached 105 kG the magnet was recharged. Therefore, the average magnetic field during the run was about 110 kG. This corresponds to an integrated field of about 1.5×10^6 G cm. At 1.80 GeV/c a magnetic moment of 1 nuclear magneton would precess in this field by about 20°. The magnet used copper ribbon as insulator. In this way when the magnet went normal, the dissipation into heat of the energy stored in the solenoid (about 50 kilojoules) took place in a time of the order of one second, reducing the problems connected with the sudden drop in field and the evaporation of helium.

The charging of the solenoid turned out to be a delicate and slow procedure. The terminals of the solenoid were connected to a dc regulated power supply; a superconducting switch, which was normally closed and shorted the two terminals, was opened by heating a piece of the superconducting wire. The charging was performed with a 20–30-mV potential. Because of the large inductance of the coil (about 18 H), the time required to reach the full magnetic field, corresponding to a current of 80 A, was about one day. The time could have been decreased by charging with a larger voltage, but the procedure was dangerous, because at high fields it was very easy to drive the magnet normal. Even charging with a large voltage at the beginning of the operation when the field was low was dangerous because of the magnet memory. Extreme care was exercised to avoid any possible voltage surge while charging the magnet.

The helium was in a closed circuit with a liquefying unit. The arrangement of the target, magnet, and helium vessel is shown in Fig. 8. The liquefier was able to supply up to 8 liters of liquid helium per hour, which was more than adequate for the experiment. Figure 9 shows the magnetic field distribution along the magnet axis.

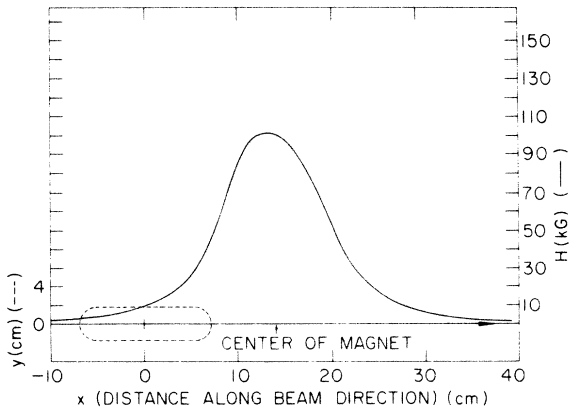

FIG. 9. The magnetic field distribution along the axis of the superconducting solenoid, normalized to 100 kG at the center. The dashed line shows the relative position of the hydrogen target.

E. K^+ detector

The electronic selection of the Ξ^-K^+ events produced in the hydrogen target was accomplished primarily by identifying the K^+ by means of a low-energy K^+ detector[8] shown in Fig. 10. The K^+ mesons were produced at large laboratory angles in association with the "forward-produced" Ξ^-. K^+ mesons from reaction (5) produced between 75° and 120° crossed the cylindrical scintillation counter R and stopped in the glycerine-filled threshold Čerenkov counter. The shaded area in Fig. 10 indicates the region where the K^+ stopped inside the counter. The index of refraction of the glycerine ($n=1.475$) is such that the K^+ mesons were too slow to produce Čerenkov radiation, but such that most of the fast mesons from the decay would radiate. A delayed count was thus required from the K^+ counter. Only those K^+ mesons were selected that lived between 5.5 and 55 nsec. The glycerine was viewed with 95 RCA 7746 photomultipliers. Signals from alternate tubes were combined to provide two outputs (K_0) and (K_e) in the following

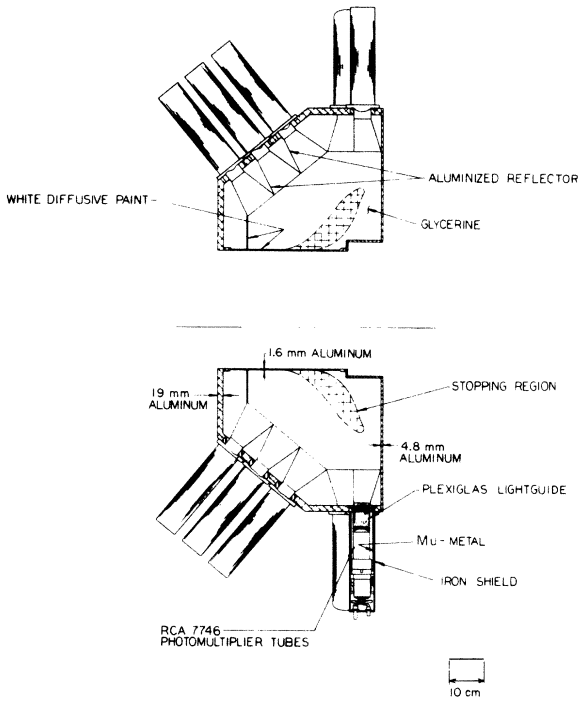

FIG. 10. Details of the K^+ detector. The shaded area denoted "stopping region" is the region where the K^+'s from the $K^-p\rightarrow K^+\Xi^-$ reaction stop inside the K^+ detector.

way. The 48 outputs of (K_0) [and the 47 of (K_e)] were added in six groups of 8 photomultipliers each by linear passive mixers, whose outputs were then added in Chronetics[9] linear mixers having net voltage gain of one. Two EG&G[10] amplifiers, each with a gain of 4, were used in cascade in each of (K_0) and (K_e). The signals were then at the correct level for triggering standard Chronetics discriminators. The effect of tube noise was made negligible by requiring a coincidence between (K_0) and (K_e). The use of $(\bar{G})$ (see Figs. 3 and 4) in anticoincidence with (K_0K_e) reduced by an order of magnitude the number of random events by eliminating the effect of the halo of particles surrounding the main beam, which went through the K^+ detector.

The performance of the K^+ detector was measured in a test run with incident K^+ mesons and a polyethylene (CH_2) target.[8] Two kinds of tests were performed. In the first type we used K^+ scattered from the target and which reached the R counter (the R counter was in prompt coincidence and the K^+ detector in delayed coincidence). In the second test the K^+ scattered and decayed inside the target (the R counter was placed in delayed coincidence with the K^+ detector).

In the first case we made attenuation curves on K_0 and K_e. The attenuation curves indicated that the voltage gains were adequate, though we never achieved a good plateau, as was expected on the basis of the decay products detected. A study of the K^+ lifetime was also made (see Fig. 11).[8]

In the second case we made an efficiency determination of the K^+ detector. The efficiency was defined as

$$\text{eff} = \frac{(K^+\bar{T}RK_0K_e\bar{G})}{(K^+\bar{T}R)}. \tag{19}$$

The measured efficiency gave the fraction of the decay products reaching the R counter, which were counted by the K^+ detector. From this number we estimated that the over-all efficiency of the K^+ detector when detecting K^+'s from the reaction $K^-p \to \Xi^-K^+$ was about 50–60%. This efficiency compares favorably with the efficiencies of other K^+ detectors.[2]

F. Electronic logic

Figure 12 shows a block diagram of the electronics used in conjunction with the layout of Fig. 4. Dimensions of all scintillation counters are shown in Table I.

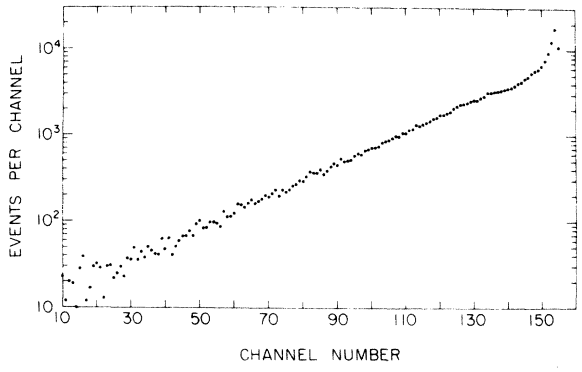

FIG. 11. K^+ lifetime distribution measured in the calibration run for the K^+ detector. The best fitted lifetime is $\tau_{K^+} = 12.44 \pm 0.05$ nsec.

All particles in the incoming beam were counted by the scintillation counter coincidence $(S) = (S_1S_2\bar{G})$. One role of $\bar{G}$, a scintillation counter with a hole for the beam defined by S_1 and S_2, was to eliminate particles outside the beam in order to reject K^- interactions in the cell of the differential Čerenkov counter and to reject accidental coincidences. The coincidence $(C) = (C_1C_2\bar{C})$ indicates the passage of a K^- meson. It was obtained after combining the outputs of the individual tubes with passive mixers as shown in Fig. 12. The mixed signals (C_1) and (C_2) were each amplified by a pair of EG&G amplifiers for a total gain of 9 before discrimination. The $(\bar{C})$ signals were mixed and then amplified by a Chronetics amplifier with a gain of 5 before discrimination. The coincidence (SC) then defined the K^- mesons in the beam.

A requirement was made that one and only one charged particle be emitted in the forward direction at the exit of the magnet. This was accomplished by adjusting the discriminators of the two dE/dx counters S_3 and S_4 so that pulses from only 30% of the single particles would exceed the threshold.

The T counters consisted of two circular scintillation counters T_{12} and T_{34}, each viewed with two photomultipliers on opposite sides of the scintillator, and one annular scintillation counter T_{567}, viewed by three photomultipliers around the circumference. The T counters required at least two charged particles. This was accomplished by requiring either coincidence between T_{12} and T_{567} or a coincidence between T_{12} and T_{34} where the thresholds on their discriminators were set at 1.5 times that for a minimum-ionizing particle. This latter selection demanded that both the Ξ^- and Λ decayed via their charged modes before reaching T.

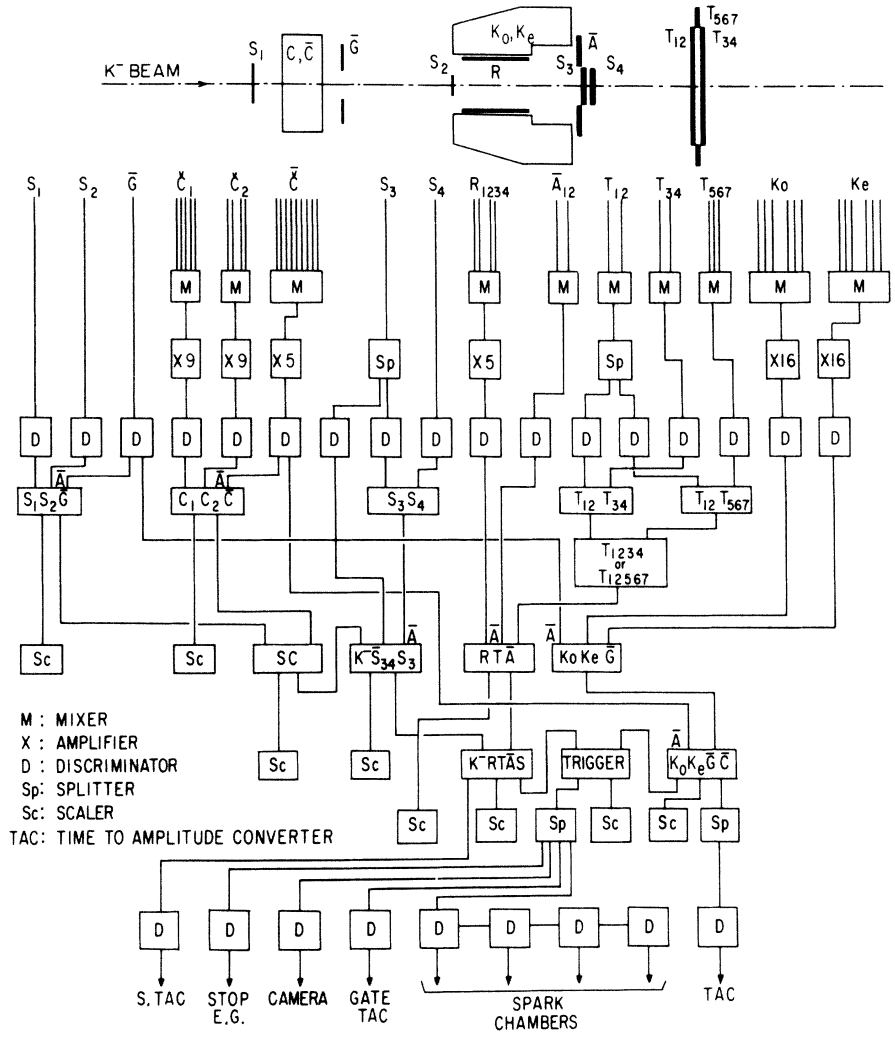

FIG. 12. Block diagram of electronics used in conjunction with the layout of Fig. 4.

In the coincidence ($RT\bar{A}$) the requirement was further made by the annular scintillation counter $\bar{A}$ that no charged particles be emitted at large angles through the superconducting magnet, and by the counter R that a charged particle enters the K^+ detector.

As has been described in Sec. III E the outputs from the 95 photomultipliers of the K^+ detector

TABLE I. Scintillation-counter dimensions

Counter	
S_1	3 in.×3.5 in., 0.125 in. thick
S_2	1.125 in. diam., 0.125 in. thick
S_3, S_4	3 in. diam., 0.25 in. thick
T	20 in. diam., 0.5 in. thick
T_{12}, T_{34}	12.25 in. diam., 0.5 in. thick
T_{567}	12.5 in. I. D., 23.5 in. O. D., 0.5 in. thick
R	8.95 in. O. D., 8.45 in. I. D., 8.25 in. long
$\bar{G}$	2 in. I. D., 24 in. O. D.
$\bar{A}$	2.375 in. I. D., 6 in. O. D., 0.125 in. thick (without magnet); 3 in. I. D., 10 in. O. D., 0.125 in. thick (with magnet)

were mixed in two groups and taken in coincidence. The $(\overline{G})$ signal as well as the $(\overline{C})$ signal were used in prompt anticoincidence with (K_0K_e) to greatly reduce the accidentals.

The prompt coincidence $(K^+RT\overline{A}S)$ signalled the presence of an interaction which gave particles of the correct geometrical form. This prompt coincidence was placed in delayed coincidence with the output of the K^+ detector $(K_0K_e\overline{G}\,\overline{C})$ thus giving what we called an "event" and triggered the spark chambers. The delay between the prompt signal and the K^+ signal was measured in a time-to-amplitude converter and a pulse-height analyzer.

G. Spark chambers and optics

Optical spark chambers were used to record the geometry of each event. They were all thin-foil aluminum chambers, with gaps of 0.6–1.2 cm. The spark chambers were arranged in the following manner (Fig. 13):

The first set of three chambers, which included a small two-gap chamber ("micro" chamber) just in front of the H_2 target, recorded the trajectory and the point of incidence at the target of the incoming K^-. The second set consisted of an 8-gap cylindrical chamber surrounding the target. This chamber registered the outgoing K^+. A 45-element fan-mirror was used to provide a 15° stereo view. The third set was placed immediately after the magnet and recorded the Ξ^-, the π^- from the Ξ^- decay, and the decay of the Λ into p and π^-. In the preliminary measurement of the polarization in Ξ^- production the magnet was replaced with a small spark chamber, in order to see those Ξ^-'s which decayed close to the target.

Figure 13 gives a plan view of the optics used. All chambers, except the cylindrical chamber, were photographed at 90° stereo. The optical path was 6 m for all chamber views. All chamber views were photographed on one 35mm frame, where other information was also displayed (chamber fiducials, frame number, magnetic field value, K^+ decay time, etc.). Figure 14 shows an event taken without the magnet.

IV. EXPERIMENTAL PROCEDURE

A. Data taking

Prior to this experiment, about 5000 Ξ^- events produced in many different final states in different bubble-chamber experiments were analyzed to determine the Ξ^- decay parameters.[11] Some of them also provided information on the polarization of the Ξ^- produced in reaction (5). The available data indicated that the polarization of the Ξ^- was

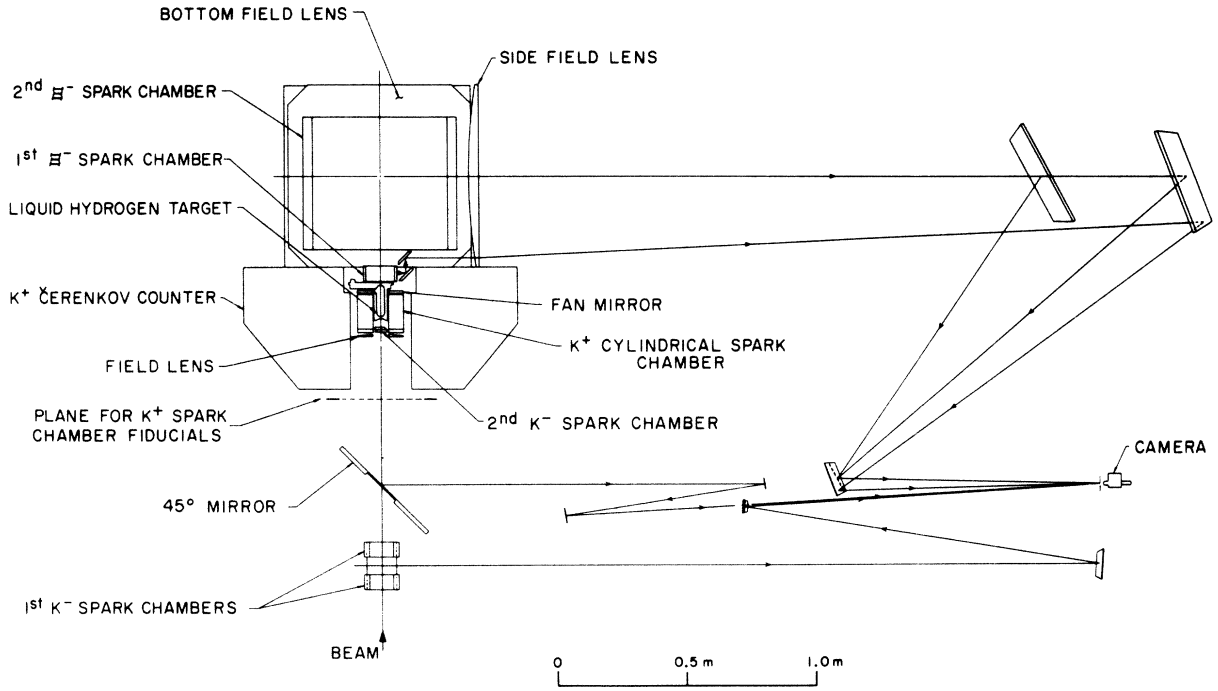

FIG. 13. Plane view of the layout of the optics for the spark chambers. A single camera was used for recording all the information.

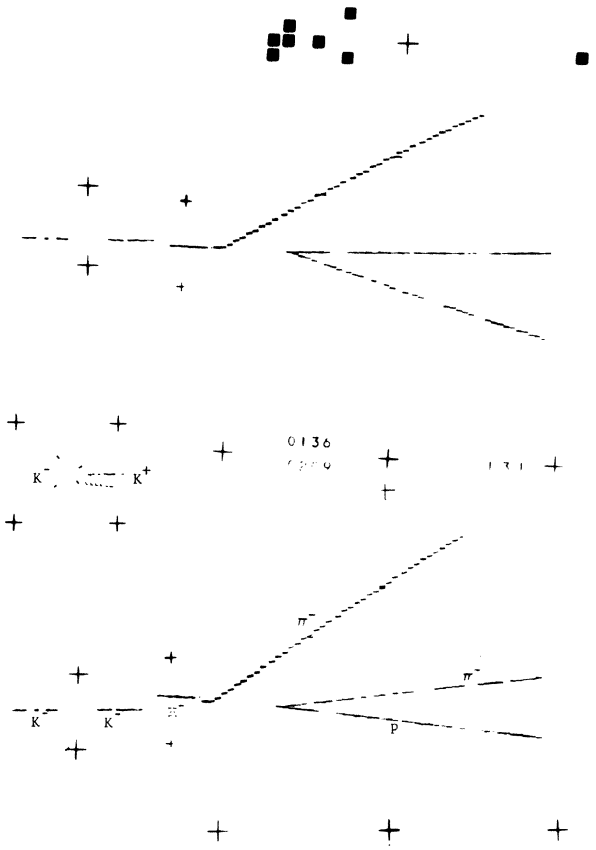

FIG. 14. Photograph of an accepted $K^-p \to K^+\Xi^-$ event taken without the magnet. The points of incidence of the K^- at the target and the K^+ track, as viewed along the beam direction, are shown on the middle left. The point of incidence of the K^- before the hydrogen target is determined by the intersection of the two 90° lines defined by the four individual sparks. The direct view of the K^+ track in the cylindrical chamber seems to originate from the point of incidence. The other track is the 15°stereo view. The two stereo views of the incoming K^- and the decays of the Ξ^- and the Λ are shown on top and bottom. The view of the K^- was moved optically towards the decay chambers. Recorded on the pictures are fiducials, frame number, and channel number of the time-to-amplitude converter related to the K^+ lifetime.

varying rapidly with K^- momentum and Ξ^- production angle. In particular it was very uncertain for Ξ^-'s produced within the angular range of about $4.2° < \theta_{lab} < 11.5°$. Thus, in the first part of this experiment data were taken at 1.74 GeV/c, 1.80 GeV/c, and 1.87 GeV/c with the magnet replaced by another spark chamber to measure the Ξ^- polarization. Subsequent runs with the magnet in place were done at 1.83 GeV/c. The magnetic field polarity was reversed frequently during the run and is defined to be positive when the field is in the direction of flight of the Ξ^-.

At the beginning of each running period the beam was focussed on S_2 and was optimized in intensity and in the K^- to π^- ratio. Checks on this optimization as well as other checks were performed regularly about once a week, while at the beginning of each new roll of film simple checks were performed to make sure that no sudden change in counting rates occurred. The following checks were made:

(i) It was required that the beam be focussed on S_2 [the ratio of beam counted as $(S_1S_2\bar{G})$ to total flux, as given by the (S_1T) rate, exceeded 70%].

(ii) A check of the K^- to π^- separation was made by repeating a curve as shown on Fig. 7. We required that at the K^- setting of the liquid differential counter the pion rate should be smaller than $\frac{1}{1000}$ of the K^- rate.

(iii) We set the trigger rate to be about 1 per AGS pulse. This was achieved by changing the delay of $(K_0K_e\bar{G})$ with respect to the prompt rate (see Sec. III F). In this condition one roll of film containing 4000 frames was exposed in about 2.5 hours.

(iv) In the runs with the magnet (set-up of Fig. 4) we made sure that the two dE/dx counters were removing the one-prong events without reducing the efficiency for two-prong events below the 95% level.

During the second series of runs the superconducting magnet was charged up to 118 kG; then in about two days the field slowly decreased to 105 kG. At this moment the magnet coil was reconnected to a dc power supply, a superconducting switch was turned off in the magnet coil, by heating a junction, and the magnet was recharged to the value of 118 kG. Laboratory tests had shown that the magnet stopped being superconducting and went normal at 122 kG. Because of voltage surges or other instabilities, the magnet went normal occasionally during runs when it was at fields smaller than 118 kG. In these cases we had to warm up the magnet to about 40 °K in order to erase its memory; then the magnet was slowly charged up in about one day to the operating field of 118 kG.

Special test runs were also performed with data taken with no hydrogen in the target. We found that the event rate went down by more than one order of magnitude. The field-on data were taken in about 600 hours of running time.

B. Scanning and measuring

A total of about 400 000 pictures were taken without the magnet and another 950 000 pictures were taken with the magnet. All pictures were scanned three times by two different scanners for

an incoming K^- track in the beam chamber, a V-shaped pattern corresponding to the Λ decay, and a straight track corresponding to the π^- from Ξ^- decay in the decay chambers. The selected events were then hand-measured using an image-plane digitizer with an accuracy of about 0.2 mm in real space. All chamber fiducials were surveyed and rechecked by straight through tracks to within 1 mm. All measured events were then processed by Brookhaven's CDC 6600 computer.

C. Geometrical and kinematical reconstruction

For the no-field case, the geometry of each event was reconstructed and checked for coplanarity on all tracks at the Ξ^- production, Ξ^- decay, and Λ decay vertices. Then a kinematics fit was done separately on each vertex to obtain the starting values for the final kinematics fit taking all the three vertices at once.

For the field-on events there was the extra problem of reconstructing the trajectories of the Ξ^- and of the K^+ in the magnetic field. The magnetic field was mapped by using a Hall probe and the values were stored in the computer. The directions at production of the K^+ and the Ξ^- were evaluated by means of a track-tracing routine. Then the previously mentioned chain of programs was used.

The K^+ track was in general curved due to the fringe field, especially in the plane normal to the beam. The direction of the K^+ track at the production vertex was determined by tracing the track through the mapped field distribution using a starting momentum determined by the polar angle of the observed track, and constrained by the observed portion of the track in the cylindrical chamber and the point of incidence of the K^- track as observed in the "micro" chamber. The tracing was repeated once more after a kinematics fit on the production vertex, using the K^+ direction obtained in the first tracing as it gave a better estimate on the K^+ momentum.

In the tracing of the Ξ^- track, the starting Ξ^- momentum was taken from the kinematics fit at the production vertex and the tracing was constrained by the production vertex and the decay vertex of the Ξ^- only. The Ξ^- and Λ decay geometry was then corrected for the small rotation resulting from this tracing. The Λ direction was obtained by weighting that calculated from the Ξ^- decay and that determined by the Ξ^- and Λ decay vertices in order to avoid the uncertainty due to a short Λ track. The momenta obtained by fitting the three single vertices individually were then used as starting values to the final over-all fit on the three vertices simultaneously.

The geometry and kinematics programs and their resolutions were checked by Monte Carlo simulation. Monte Carlo events were generated and points were taken on each track as if from the measuring table. Gaussian errors were given to these points, consistent with measuring errors. These coordinates were then used as input to the reconstruction programs as for real events.

The Monte Carlo events were generated according to the known Ξ^- angular distribution at production, according to the decay kinematics, and taking into account the geometry of the experiment. The generation did not take into account the beam divergence, nor the beam momentum resolution, nor attenuation or scattering in the target.

The Monte Carlo simulation allowed a number of tests to be made:

(1) Check of the track-tracing routines for the K^+ and the Ξ^- in the magnetic field. The test revealed the importance of knowing accurately the momentum of the K^+ track. It allowed a determination of the accuracy in determining the K^+ azimuthal angle (full width at half maximum of 4° before the final 3-vertex fit and 3° after the fit) and the Ξ^- rotation angle (FWHM of 0.8°). For the K^+ track the dispersion of the azimuthal angle was symmetric about 0° (see Fig. 15), and no bias was introduced by the tracing.

(2) Check of the reconstruction and fitting programs for possible biases and program efficiency. It was found that because of the small forward angles involved, the Λ direction could not be determined with enough accuracy by the two decay vertices especially for short Λ track, but that one had to use the procedure already described. Otherwise a bias on the very forward-going Λ will be introduced. It was also found that if one used events

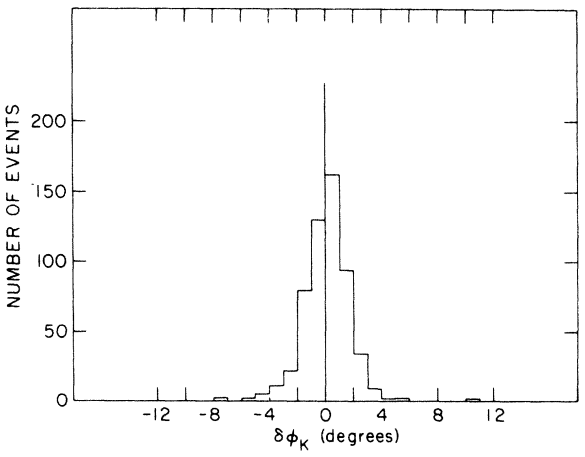

FIG. 15. Distribution of the difference in the K^+ azimuthal angle between the fitted and the Monte Carlo events at 100 kG. Note that the distribution is centered at 0°; the width of the distribution corresponds to the resolution of the measurement.

without a visible K^+, the $\hat{\sigma}_\Xi$ could have an apparent rotation. Events with a visible K^+ track, but without any K^- track on the "micro" chamber just ahead of the hydrogen target gave no bias in $\hat{\sigma}_\Xi$, but broadened the azimuthal angle distribution.

The acceptance on the Monte Carlo events by the reconstruction and fitting programs was about 92% on the first fit, and was up to 97% after a second fit to the remeasured rejected events. As an overall check we also fed into the programs Monte Carlo events corresponding to known decay parameters and Ξ^- magnetic moment and checked that they gave back the same answers.

(3) Corrections on Ξ^- and Λ lifetimes. The lifetime distributions of Ξ^- and Λ were corrected with the Monte Carlo events for inefficiencies in detecting both short and long decays due to the finite target size.

A total of 1920 events with no field and 1700 events with field, both with the Ξ^- decaying in the chamber, were accepted by the reconstruction and fitting programs. Events were further selected according to the following criteria: (1) There was a K^+ track in the cylindrical chamber, (2) the "micro" chamber shows the point of incidence, (3) the separation between the Ξ^- and Λ decay vertices was more than two gaps, and (4) the over-all fit $\chi^2 \leq 20$. After the selection, 1302 no-field events and 1134 field-on events remained which were used in the final analysis. Figure 16 shows the Ξ^- production angular distributions for this sample.

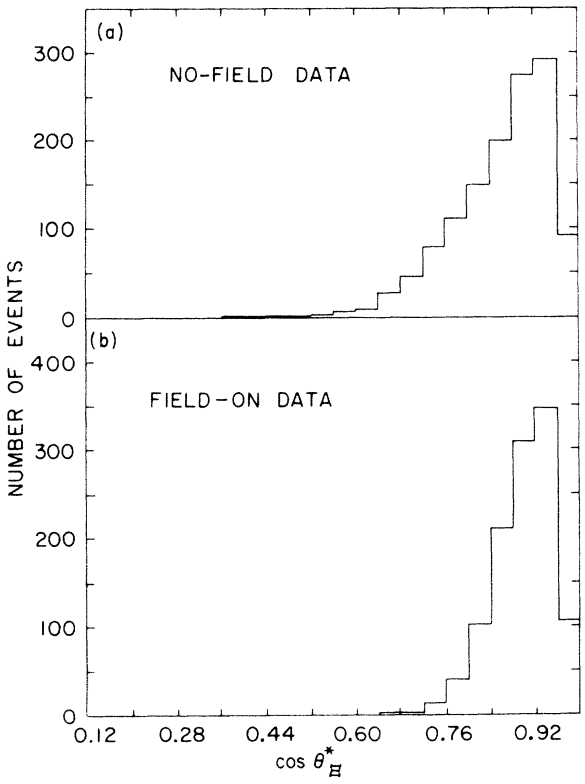

FIG. 16. The angular distributions of the Ξ^- in the production center-of-mass system for (a) no-field events, and (b) field-on events. The narrower angular distribution of the field-on data is due to the smaller angular acceptance.

V. DATA ANALYSIS AND RESULTS

A. Lifetimes and $\alpha_\Lambda \alpha_\Xi$

For the selected samples of events we computed the K^+, Ξ^-, and Λ lifetimes. They were corrected

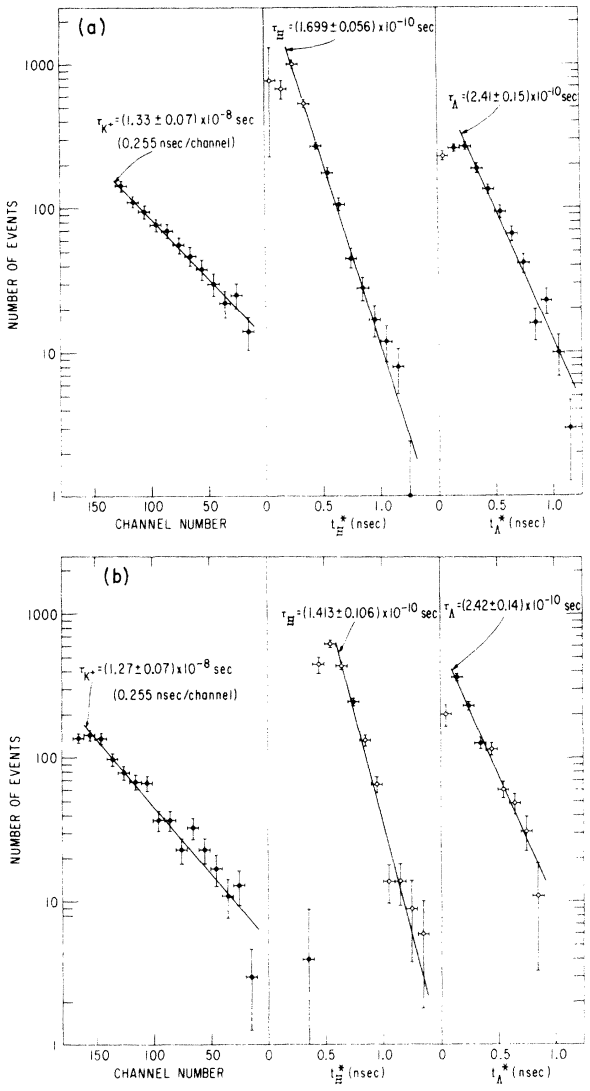

FIG. 17. K^+, Λ, and Ξ^- lifetime distributions for (a) no-field events, and (b) field-on events. Points with open circles were corrected for finite target size and long decay path. The points beyond the lines were not used in the fits.

TABLE II. Results of the χ^2 fits to the lifetime distributions of K^+, Ξ^-, and Λ, and to the $(\hat{p}\cdot\hat{\Lambda})_\Lambda$ distributions.

	τ_{K^+} (10^{-8} sec)	τ_Λ (10^{-10} sec)	τ_{Ξ^-} (10^{-10} sec)	$\alpha_\Lambda\alpha_\Xi$
From no-field events	1.33 ± 0.07	2.41 ± 0.15	1.699 ± 0.056	−0.262 ± 0.047
From field-on events	1.27 ± 0.07	2.42 ± 0.14	1.413 ± 0.106	−0.260 ± 0.057
Weighted average	1.29 ± 0.05	2.42 ± 0.10	1.637 ± 0.050	−0.261 ± 0.037
Previous accepted value (Ref. 11)	1.2371 ± 0.0026	2.521 ± 0.021	1.672 ± 0.032	−0.259 ± 0.021

for the effect of finite target size using Monte Carlo simulation as mentioned above. The results are shown in Fig. 17. The losses of the short-lived Ξ^- and Λ events were due to scanning inefficiency. The loss of the short-lived K^+ events was due to the electronic gate jitter. The fitted results, as shown in Table II, are in good agreement with the published values.[11] This shows that with our criteria a clean sample of reaction (5) was selected. To check the no-field and field-on events, we compared the only field-independent distribution of $(\hat{p}\cdot\hat{\Lambda})_\Lambda$ from both samples as shown in Fig. 18. A fit to Eq. (15) gave the values of $\alpha_\Lambda\alpha_\Xi$ as shown in Table II. The two values are in excellent agreement with each other and with the published value.[11]

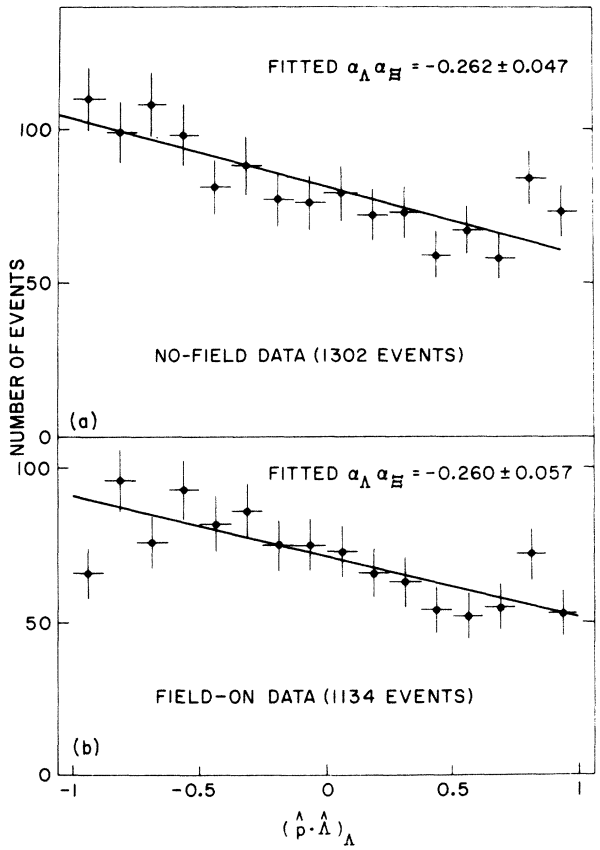

FIG. 18. The $(\hat{p}\cdot\hat{\Lambda})_\Lambda$ distributions for (a) no-field events, and (b) field-on events. The lines are the results of a χ^2 fit to Eq. (15).

B. Decay parameters and polarizations from no-field data

The angular distributions $(\hat{\Lambda}\cdot\hat{\sigma}_\Xi)_\Xi$, $(\hat{p}\cdot\hat{\Lambda})_\Lambda$, $(\hat{p}\cdot\hat{y}')_\Lambda$, $(\hat{p}\cdot\hat{z}')_\Lambda$, and $(\hat{p}\cdot\hat{\sigma}_\Xi)_\Lambda$ were computed for the no-field sample. They are shown in Figs. 18 and 19. For each momentum they were first fitted using the minimum χ^2 method to Eqs. (14)–(18) to give starting values to a maximum-likelihood fit which yielded the decay parameters and polarizations. The results are shown in Table III. These results were obtained by fixing $\alpha_\Lambda = 0.645$ (Ref. 11) with no error. As a check, α_Λ was also varied in these fits and the results remained unchanged.

C. Decay parameters, polarizations and magnetic moment from all data

1. *Rotations of the projected decay distributions*

In a magnetic field which precesses the polarization vector by an angle ϵ, it is useful, for illustrative purposes and for a qualitative assessment of the data, to examine the distributions obtained by projecting the distributions (14) and (18) onto the plane perpendicular to the Ξ^- momentum. With η the appropriate projected angle we have

$$D_i(\eta) \propto [\,1 + \tfrac{1}{4}\pi A_i \cos(\eta - \epsilon)\,], \quad i = 1, 5 \tag{20}$$

where

$$A_1 \equiv \alpha_\Xi \overline{P}\,, \qquad A_5 \equiv \tfrac{1}{3}(1+2\gamma_\Xi)\alpha_\Lambda \overline{P}\,. \tag{21}$$

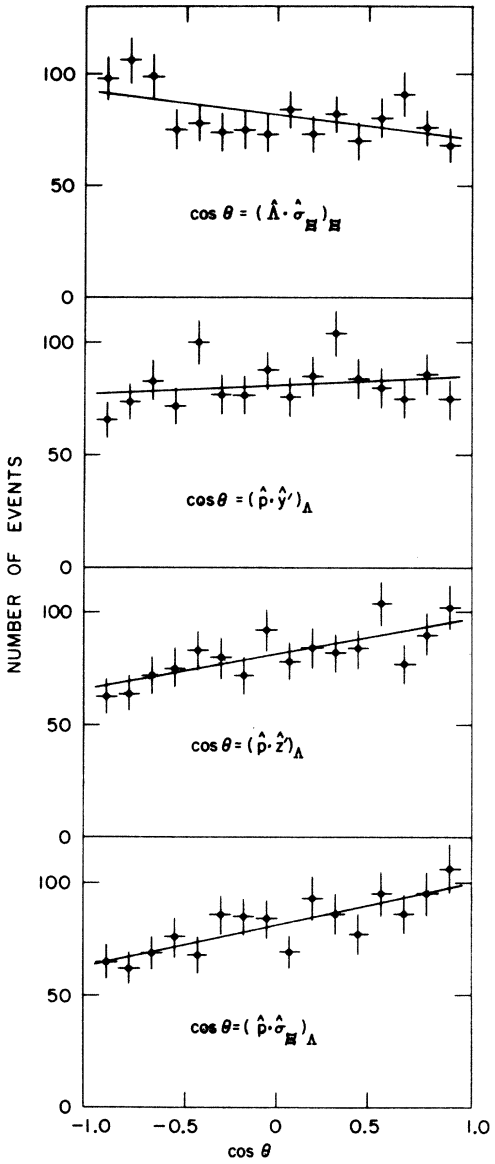

FIG. 19. The decay angular distributions for the no-field events. The lines are the results from χ^2 fits to Eqs. (14) and (16)–(18). The corresponding maximum-likelihood results are shown in Table III.

Thus, in the projected distributions (20) the effect of the precession is simply to rotate the distributions by the precession angle ϵ.

It is convenient to use the normalized left-right asymmetry R as defined below:

$$R \equiv \frac{N_R - N_L}{N} = \tfrac{1}{2} A \sin(\delta - \epsilon), \tag{22}$$

where

$$N_R \equiv \int_{\delta}^{\delta+\pi} D(\eta)d\eta = \tfrac{1}{2}N[\,1 - \tfrac{1}{2}A\sin(\delta-\epsilon)\,],$$
$$N_L \equiv \int_{\delta+\pi}^{\delta+2\pi} D(\eta)d\eta = \tfrac{1}{2}N[\,1 + \tfrac{1}{2}A\sin(\delta-\epsilon)\,], \tag{23}$$

N is the total number of events, δ is the angle measured in the plane normal to the Ξ^- direction and is 0 at the direction $\hat{\sigma}_{\Xi^-}$, and A is equal to A_1 or A_5 depending on which distribution is used.

In Fig. 20 we plotted the left-right asymmetry R with respect to an axis rotated in the projected plane for both the Ξ^- and Λ decays under each of the three (+, −, 0) field conditions. R should pass through zero at an angle equal to ϵ.[2] These distributions were fitted to Eq. (22) and the results are shown in Table IV. These fitted results were used as starting values for a number of maximum-likelihood fits as described below. Within statistics, the data show the correct behavior; namely, (1) for each distribution ϵ reverses sign with reversal of the magnetic field, (2) the zero-field distributions are consistent with $\epsilon = 0$, and (3) the amplitude and relative phase of the Ξ^- and Λ distributions are consistent with the known signs and values of α_{Ξ}, α_{Λ}, and γ_{Ξ}.

Figure 21 shows for each field configuration the distribution obtained by combining the distribution (14) and (18).

2. *Maximum-likelihood fit to the projected decay distributions*

In order to make maximum use of all data and to include the effects of the field integral and the Ξ^-

TABLE III. Results of Ξ^- decay parameters and polarizations from maximum-likelihood fits to the no-field data. In the fit α_Λ was assumed to be 0.645 without error.

K^- momentum (GeV/c)	Number of events	α_{Ξ}	β_{Ξ}	γ_{Ξ}	ϕ_{Ξ} (deg)	$\bar{P}_1$	$\bar{P}_2$	$\bar{P}_3$
1.74	404	−0.48 ± 0.13	−0.26 ± 0.43	0.84 ± 0.12	−17 ± 29	0.28 ± 0.10		
1.80	474	−0.37 ± 0.09	0.47 ± 0.33	0.80 ± 0.16	33 ± 23		0.47 ± 0.10	
1.87	424	−0.28 ± 0.11	0.56 ± 0.29	0.78 ± 0.16	41 ± 23			0.43 ± 0.12
1.74, 1.80, 1.87 combined	1302	−0.38 ± 0.06	0.31 ± 0.24	0.87 ± 0.08	20 ± 16	0.28 ± 0.10	0.45 ± 0.10	0.38 ± 0.10

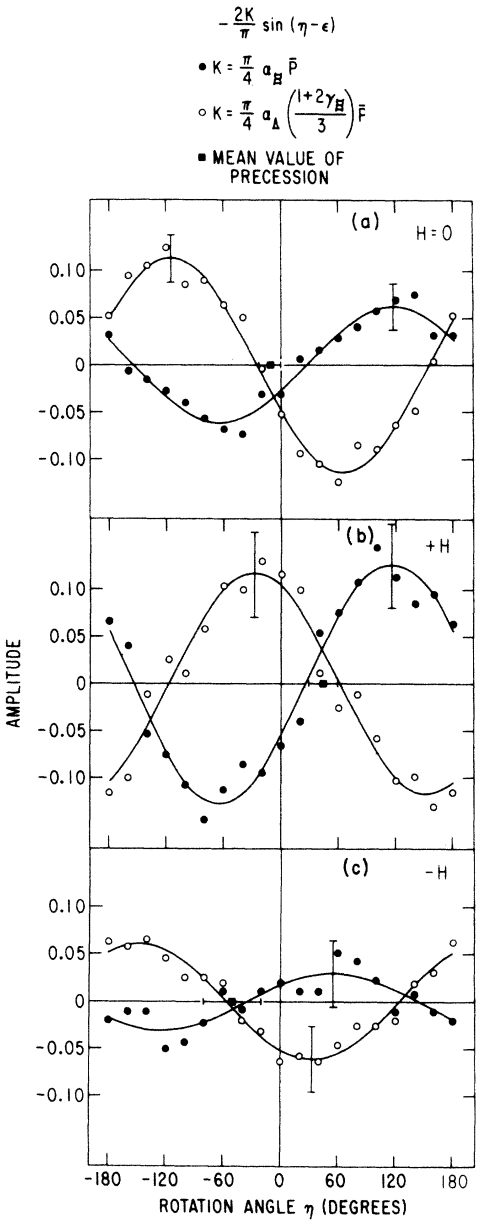

FIG. 20. The left-right decay asymmetry distributions from the Ξ^- and Λ decays for (a) no-field events, (b) positive-field events, and (c) negative-field events. The curves are the results from χ^2 fits to the asymmetry R as defined in Eq. (22).

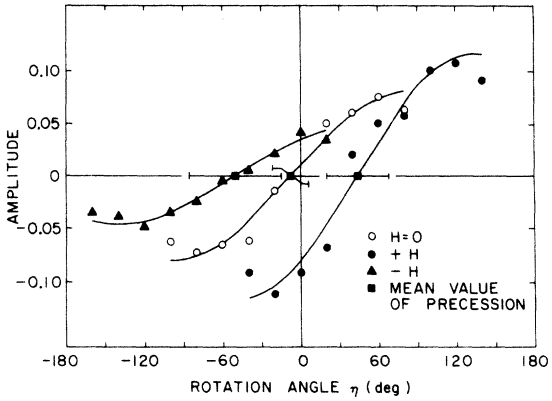

FIG. 21. Angular distributions from combining the Ξ^- and Λ decay distributions for the no-field, negative-field, and positive-field configurations. The curves are the results from χ^2 fits. The points where the curves cross the horizontal axis give the precession angle of the Ξ^- polarization direction.

momentum distributions on the magnetic moment, the final results were obtained by maximum-likelihood fits. For the projected distribution (20), the likelihood function is

$$\mathfrak{L}=\prod_{i=1}^{N} D_{1i}D_{5i}, \tag{24}$$

where

$$D_{1i}=1+\tfrac{1}{4}\pi A_1\cos(\eta_{1i}-\epsilon_i),$$
$$D_{5i}=1+\tfrac{1}{4}\pi A_5\cos(\eta_{5i}-\epsilon_i), \tag{25}$$

$$\epsilon_i\cong -1.8307\times10^{-5}(Hl)_i\frac{m_{\Xi}}{(p_{\Xi})_i}\mu_{\Xi}(\text{degrees}). \tag{26}$$

(Hl) in gauss-cm is the field integral; m_{Ξ} is the Ξ^- mass; (p_{Ξ}) is the Ξ^- laboratory momentum and μ_{Ξ} is the Ξ^- magnetic moment in nuclear magnetons. The sign is chosen such that a negative μ_{Ξ} will give a right-hand rotation around the positive field direction. The different data samples were fitted with only two parameters, $\bar{P}$ and μ_{Ξ}. We assumed $\alpha_{\Lambda}=0.645$, $\alpha_{\Xi}=-0.40$, and $\gamma_{\Xi}=0.91$ without errors. The results are shown in Table V.

TABLE IV. Results from the R distribution fits [Eq. (22)].

	From Ξ^- decay		From Λ decay		Weighted averages	
Data sample	ϵ (deg)	$\bar{P}$	ϵ (deg)	$\bar{P}$	ϵ (deg)	$\bar{P}$
Positive field	25±21	0.63±0.21	62±21	0.39±0.18	43±15	0.49±0.14
Negative field	−35±55	0.15±0.17	−58±38	0.20±0.14	−51±31	0.18±0.11
Weighted average					45±14	0.30±0.09
No field	26±24	0.31±0.13	−25±14	0.38±0.10	−12±12	0.35±0.08

TABLE V. Results for the Ξ^- magnetic moment from the two-parameter maximum-likelihood fits to the projected distributions assuming $\alpha_\Lambda = 0.645$, $\alpha_\Xi = -0.40$, and $\gamma_\Xi = 0.91$ without errors.

Sample	Number of events	$\alpha_\Xi \bar{P}$	$\bar{P}$	μ_Ξ (μ_N)
No field	1302	-0.135 ± 0.027	0.34 ± 0.07	0.4 ± 0.6[a]
Negative field	698	-0.063 ± 0.037	0.16 ± 0.09	-2.1 ± 1.7
Positive field	436	-0.161 ± 0.046	0.40 ± 0.12	-2.3 ± 0.9
All data combined	2436	-0.119 ± 0.020	0.30 ± 0.05	-2.2 ± 0.8

[a]Assuming a positive field with same average field integral as the field-on data.

3. Maximum-likelihood fit to all distributions

In a magnetic field, all the distributions (14)–(18), with the exception of (15), which is independent of the field, will follow the precession of the Ξ^- polarization vector. The modified functions, though complicated, can be expressed in terms of the precession angle ϵ and the directions of the Λ and the p ($\hat{\Lambda}$ and $\hat{p}$, respectively). Explicitly, the precessed distribution functions are

$$I_1' \propto 1 + A_1(\cos\theta\cos\epsilon - \sin\theta\sin\phi\sin\epsilon), \tag{27}$$

$$I_2' \propto 1 + A_2 p_x, \tag{28}$$

$$I_3' \propto 1 + A_3[-(\sin\theta\sin\phi\cos\epsilon + \cos\theta\sin\epsilon)p_x + (\sin\theta\cos\phi\cos\epsilon)p_y + (\sin\theta\cos\phi\sin\epsilon)p_z]/\sin\theta', \tag{29}$$

$$I_4' \propto 1 + A_4[-(\cos\theta'\sin\theta\cos\phi)p_x - (\cos\theta'\sin\theta\sin\phi + \sin\epsilon)p_y + (-\cos\theta'\cos\theta + \cos\epsilon)p_z]/\sin\theta', \tag{30}$$

$$I_5' \propto 1 + A_5(\cos\epsilon\, p_z - \sin\epsilon\, p_y), \tag{31}$$

where A_1 and A_5 are defined in (21) and

$$A_2 \equiv \alpha_\Lambda \alpha_\Xi,$$
$$A_3 \equiv \tfrac{1}{4}\pi\alpha_\Lambda\beta_\Xi\bar{P}, \tag{32}$$
$$A_4 \equiv \tfrac{1}{4}\pi\alpha_\Lambda\gamma_\Xi\bar{P},$$

$$\cos\theta' = \cos\theta\cos\epsilon - \sin\theta\sin\phi\sin\epsilon, \tag{33}$$

$$0° \leq \theta' \leq 180°.$$

(θ, ϕ) is the direction of $\hat{\Lambda}$ in the Ξ^- c.m. system, p_x, p_y, p_z are the direction cosines of $\hat{p}$ in the Λ c.m. system, and ϵ is expressed in terms of μ_Ξ as in (26).

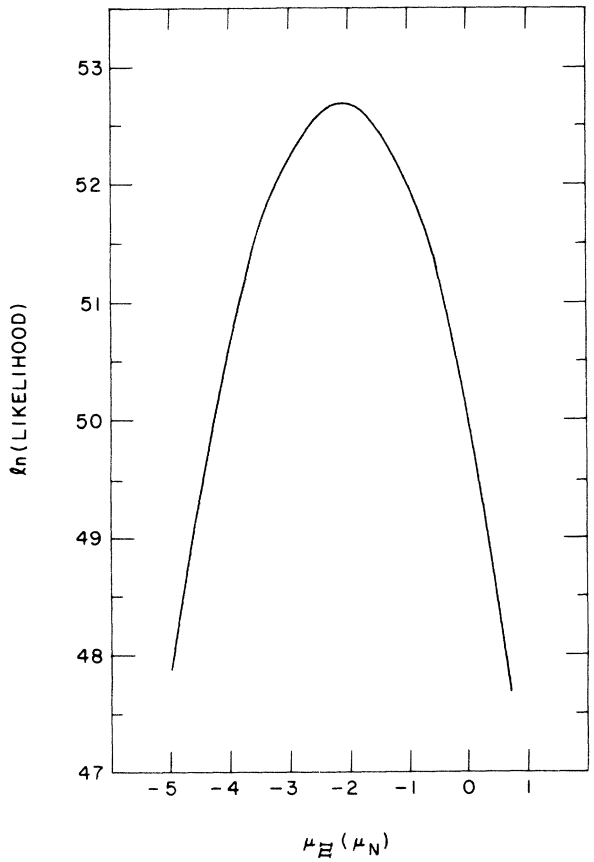

FIG. 22. Likelihood curve from combining all decay distributions.

TABLE VI. Final results from the over-all maximum-likelihood fits to all the data. α_Ξ, β_Ξ, and σ_Ξ are related by Eq. (12). $\bar{P}_1$, $\bar{P}_2$, $\bar{P}_3$, and $\bar{P}_4$ are respectively the average polarization at 1.74, 1.80, 1.87, and 1.83 GeV/c.

Number of fitted parameters	Number of events	α_Ξ	β_Ξ	γ_Ξ	$\bar{P}_1$	$\bar{P}_2$	$\bar{P}_3$	$\bar{P}_4$	μ_Ξ (μ_N)	ϕ_Ξ (deg)
						$\bar{P} = 0.29 \pm 0.04$				
4	2436	-0.38 ± 0.05	-0.05 ± 0.25	0.92 ± 0.02					-2.1 ± 0.8	3 ± 16
7	2436	-0.39 ± 0.05	0.08 ± 0.26	0.92 ± 0.03	0.29 ± 0.10	0.44 ± 0.09	0.36 ± 0.10	0.21 ± 0.06	-2.1 ± 0.8	5 ± 16
Previously accepted values (Ref. 11)		-0.40 ± 0.03		0.91						-4 ± 8

The likelihood function can then be formed using these distribution functions. Maximum-likelihood fits were performed using simultaneously all the distributions, changing the number of independent parameters to be fitted. The data were first assumed to be taken at the same momentum, so there are four independent parameters, α_Ξ, β_Ξ, $\bar{P}$, and μ_Ξ, to be fitted. In the most general case we left free the four Ξ^- polarizations at the four measured momentum so there are seven independent parameters, α_Ξ, β_Ξ, $\bar{P}_1$, $\bar{P}_2$, $\bar{P}_3$, $\bar{P}_4$, and μ_Ξ, to be fitted. In all cases, we assumed $\alpha_\Lambda = 0.645$ without error. The results are shown in Table VI. The likelihood curve is shown in Fig. 22. These should be considered to be the best determination of the decay parameters, the polarizations, and the μ_Ξ. The results as obtained from different data samples and using different analyses are all consistent within errors. The decay parameters are in very good agreement with the published values.[11] For comparison with the theory, the result of the μ_Ξ is expressed in nuclear magnetons assuming the spin of the Ξ^- to be $\frac{1}{2}$. In fact, the experiment measures the gyromagnetic ratio which is $g_\Xi = 4.2 \pm 1.6$.

V. DISCUSSION

Table VII lists a number of predictions for the Ξ^- magnetic moment.[1,4,12,13] The table indicates how a measurement of the magnetic moment could separate among various symmetries. In particular, SU(3) symmetry without mass breaking predicts a value $\mu_\Xi = -(\mu_n + \mu_p) = -0.9$ nuclear magnetons. Our value agrees in sign and is 1.5 standard deviations larger. On the other hand, since m_Ξ is nearly 40% greater than m_p the presence of an appreciable mass correction term would not be surprising. At present no fully acceptable calculation of this term is available. Only one other measurement of the magnetic moment of the Ξ^- hyperon has been reported.[14] Its value of $\mu_\Xi = (-0.1 \pm 2.1)\mu_N$ is, within its large error, consistent with our measurement.

Note added in proof. The Ξ^- decay parameters and lifetime measured in this experiment are in excellent agreement with those of a recent experiment by C. Baltay, A. Bridgewater, W. A. Cooper, L. K. Gershwin, M. Habibi, M. Kalelkar, N. Yeh, and A. Gaigalas [Phys. Rev. D 9, 49 (1974)] which gave $\alpha_\Xi = -0.376 \pm 0.038$, $\phi_\Xi = 11^\circ \pm 9^\circ$, and $\tau_\Xi = (1.63 \pm 0.03) \times 10^{-10}$ sec.

ACKNOWLEDGMENTS

We wish to thank W. P. Sampson and his group at the BNL Accelerator Department for building the

TABLE VII. Experimental values and various predictions for the magnetic moments of the members of the $\frac{1}{2}^+$ baryon octet. The magnetic moments are in units of nuclear magnetons. One of the values is corrected for symmetry breaking.

Particle	Experimental value (μ_N)[a]	SU(3) prediction[b]	SU(3) integral charges[c]	Global symmetry[d]
P	$2.792\,782 \pm 0.000\,017$	input	input	input
n	$-1.913\,148 \pm 0.000\,066$	input	input	input
Λ	-0.67 ± 0.06	$-0.95 = \frac{1}{2}\mu_n$	$-1.59 = \frac{5}{6}\mu_n$	0
Σ^+	$+2.59 \pm 0.46$	$2.79 = \mu_p$	$2.79 = \mu_p$	$2.79 = \mu_p$
Σ^0	?	$+0.95 = \frac{1}{2}\mu_n$	$-0.95 = \frac{1}{2}\mu_n$	0
Σ^-	$-1.6 < \mu_{\Sigma^-} < 0.8$[e]	$-0.88 = -(\mu_n + \mu_p)$	$-4.70 = \mu_n - \mu_p$	$-2.79 = -\mu_p$
Ξ^-	-1.9 ± 0.8[f]	$-0.88 = -(\mu_n + \mu_p)$	$-4.70 = \mu_n - \mu_p$	$-2.79 = -\mu_p$
Ξ^0	?	$-1.91 = \mu_n$	$-1.91 = \mu_n$	$1.91 = -\mu_n$

[a]Reference 11.
[b]Reference 1.
[c]Reference 12.
[d]Reference 13.
[e]J. D. Fox, W. C. Lam, P. D. Barnes, R. A. Eisenstein, J. Miller, R. B. Sutton, D. A. Jenkins, M. Eckhause, J. R. Kane, B. L. Roberts, R. E. Welsh, and A. R. Kunselman, Phys. Rev. Lett. 31, 1084 (1973).
[f]This value is the weighted average between the result of Ref. 14 and the result of this experiment.

superconducting magnet. We also wish to thank J. Sanford and the AGS staff for their cooperation. The technical assistance of G. Munoz, F. Seir, H. Sauter, and O. Thomas and the untiring efforts of our scanners, M. L. Montecalvo, R. Gianopoulos, R. Arata, and G. Isherwood, are greatly appreciated.

---

*Work performed under the auspices of the U. S. Atomic Energy Commission.
†Present Address: The Rockefeller University, New York, New York.
‡On leave of absence from the University of Bologna, Bologna, Italy.
§Present Address: University of Arizona, Tucson, Arizona.
‖Present Address: Institute of Physics, University of Zagreb, Zagreb, Yugoslavia.
¶Present Address: Centre d'Etudes Nucléaires, Saclay, France.

[1]S. Coleman and S. L. Glashow, Phys. Rev. Lett. 6, 423 (1961).
[2]R. L. Cool, E. W. Jenkins, T. F. Kycia, D. A. Hill, L. Marshall, and R. A. Schluter, Phys. Rev. 127, 222 (1962); D. A. Hill, K. K. Li, E. W. Jenkins, T. F. Kycia, and H. Ruderman, Phys. Rev. Lett. 15, 85 (1965); Phys. Rev. D 4, 1979 (1971).
[3]R. L. Cool, G. Ciacomelli, E. W. Jenkins, T. F. Kycia, B. A. Leontic, K. K. Li, and J. Teiger, Phys. Rev. Lett. 29, 1630 (1972).
[4]T. D. Lee and C. N. Yang, Phys. Rev. 108, 1645 (1957); W. B. Teutsch, S. Okubo, and E. C. G. Sudarshan, Phys. Rev. 114, 1148 (1959); Y. Ueda and S. Okubo, Nucl. Phys. 49, 345 (1963).
[5]B. Barish and T. F. Kycia, BNL internal report, 1968 (unpublished).
[6]B. A. Leontic and J. Teiger, BNL Report No. 50031, 1966 (unpublished).
[7]The magnet was designed and built by W. P. Sampson at BNL.
[8]G. Giacomelli, T. F. Kycia, K. K. Li, and J. Teiger, Rev. Sci. Instrum. 38, 1408 (1967).
[9]Chronetics Inc., Mt. Vernon, N. Y.
[10]E.G.&G., Inc., Boston, Mass.
[11]Particle Data Group, Rev. Mod. Phys. 45, S1 (1973).
[12]N. Nauenberg, Phys. Rev. 135, B1047 (1965).
[13]S. N. Biswas, Phys. Rev. 127, 1350 (1962).
[14]G. McD. Bingham, V. Cook, J. W. Humphrey, O. R. Sander, R. W. Williams, G. E. Masek, T. Maung, and H. Ruderman, Phys. Rev. D 1, 3010 (1970).

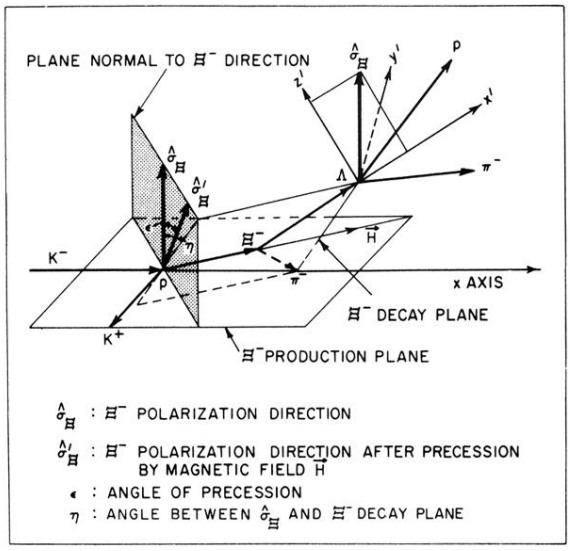

FIG. 2. Illustration of the relative orientations of the Ξ^- spin, the magnetic field, the Ξ^- momentum, and the Ξ^- cascade decay geometry.

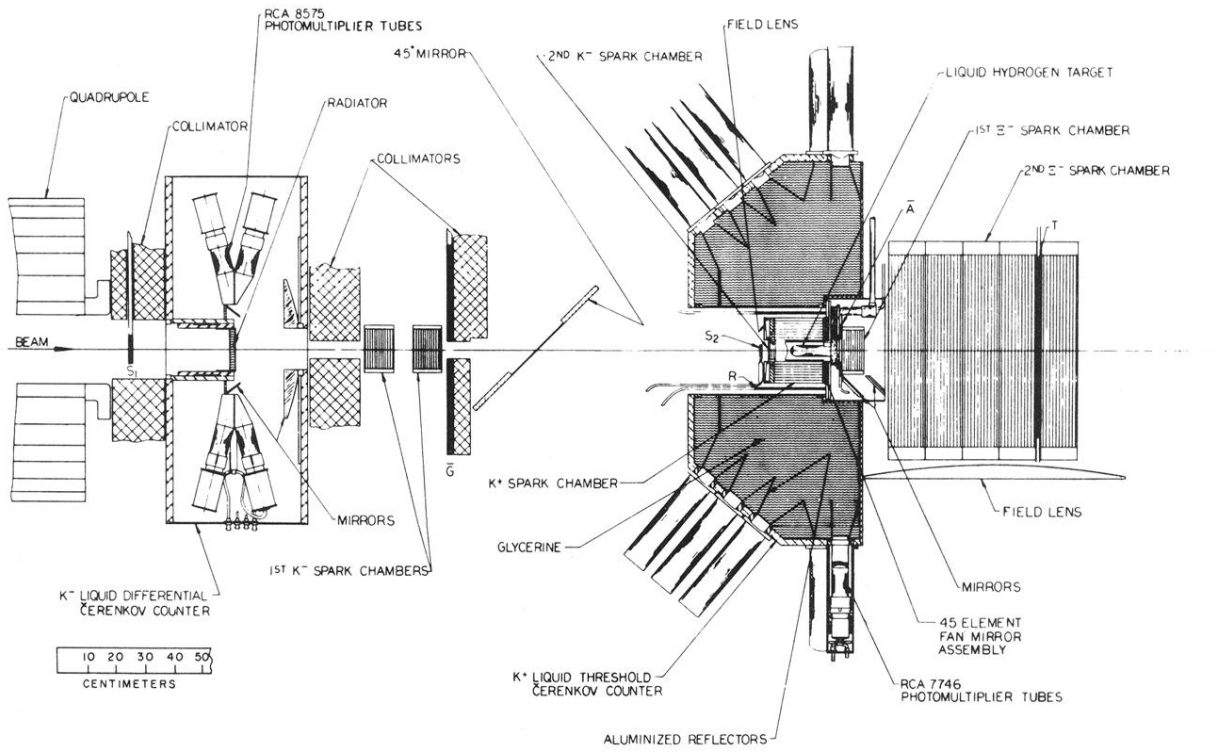

FIG. 3. Layout of the Ξ^- polarization measurements (without magnet) at 1.74, 1.80, and 1.87 GeV/c. S_1, $\overline{G}$, S_2, R, $\overline{A}$, T are scintillation counters. Also shown are the liquid differential Čerenkov counter used to select the incoming K^-, and the K^+ detector to select the K^+ decays into fast particles. The first and second K^- spark chambers were used to measure the incoming K^- direction, the cylindrical K^+ spark chamber to detect the outgoing K^+, and the first and second Ξ^- spark chambers to detect the Ξ^- production and the Ξ^- and Λ decays.